

# ESTIMATING SPACE DEBRIS DENSITY USING BEAM PARK MEASUREMENTS

F. Hermann<sup>(1)</sup>, J. Vierinen<sup>(2)</sup>, D. Kastinen<sup>(3)</sup>, J. Kero<sup>(3)</sup>, J. Markkanen<sup>(4)</sup>, and T. Grydeland<sup>(5)</sup>

<sup>(1)</sup>Karlsruhe Institute of Technology, Germany

<sup>(2)</sup>University of Tromsø, The Arctic University of Norway, [jvi019@uit.no](mailto:jvi019@uit.no)

<sup>(3)</sup>Swedish Institute for Space Physics, Sweden

<sup>(4)</sup>EISCAT Scientific Association, Finland

<sup>(5)</sup>NORCE, Norway

## ABSTRACT

Estimating the number density of space debris objects as a function of orbital elements and size is crucial for determining the risks associated with space flight. For objects  $\approx 1$  cm or larger in diameter, this information can be obtained using beam park observations made with powerful ground-based radars. This study presents a novel technique for estimating the number density of space debris objects as a function of orbital elements using the framework of statistical inverse problems. Prior information about the size and eccentricity distributions can be used to constrain the estimation problem. An important component of the presented estimation technique is the accurate modeling of the expected number of detections made by radar as a function of observed range, Doppler velocity and signal-to-noise ratio. The method is applied to the historical record of EISCAT high power large aperture radar measurements to study the evolution of the space debris environment.

Keywords: beam park, radar, space debris, density function.

## 1. INTRODUCTION

Radar beam park measurements are currently the primary method for obtaining information on space debris objects within the size range between 1 cm and 10 cm, as those are too small and too numerous to currently track and catalog using ground-based space surveillance networks, and too large and infrequent to be observed using crater counting of space flown surfaces. Beam park observations are therefore an important source of information for validating statistical models of space debris [LJF04, BHL<sup>+</sup>21]. For a review of radar beam park measurements, please refer to [MMP<sup>+</sup>21] and references therein.

The EISCAT Scientific Association currently maintains three radar systems with transmitters in Northern Norway. These radars have been used for monitoring the

space debris population for over 20 years [MLL05], with measurements covering most of the major fragmentation events, such as the 2007 FY-1C anti-satellite missile test [MJK09], the 2009 Iridium-Cosmos collision [VMK09], the 2019 Microsat-R anti-satellite missile test [Pau21], and the 2021 Cosmos 1408 anti-satellite missile test [KVGK23].

Until now, EISCAT measurements have been compared to the ESA MASTER model of space debris using the PROOF model [KBKB<sup>+</sup>00], which simulates a beam-park measurement using a debris population model. This allows a comparison of a predicted beam park observation with the actual measurement.

In this study, we propose a novel approach for space object model validation. We outline a statistical framework for inferring the number density of space objects as a function of orbital parameters from radar beam park measurements. A recently developed radar sensor model for the EISCAT radars [KVK<sup>+</sup>19, VKM<sup>+</sup>19] is used to determine the statistical distribution of observable variables in an observation period as a function of the population density. This provides us with a forward model from debris density to a beam park observation, which is inverted to determine the population density.

## 2. DATA

The data used for this study is obtained from the EISCAT UHF 930 MHz high power large aperture radar, located in Ramfjordmoen, Northern Norway. We used the *leo* experiment that utilizes a peak power of  $\approx 2$  MW, a duty-cycle of 9.6%, and 1920  $\mu$ s long binary phase coded pulses with 20 ms interpulse periods. These radar measurements were analyzed using a coherent integration based filter bank of range, range-rate, and acceleration matched filters [MLL05] that ingested 0.2 s of measurement into each detection. The radar antenna was pointed to 90° azimuth and 75° elevation, which is customary for beam park measurements, in order to obtain information about inclination from Doppler shift [SKT<sup>+</sup>95].

Table 1. Overview of the measurements used in this study. Each row represents an observation with the EISCAT UHF radar with a duration of 24 h on the specified date. The second column specifies the number of detection events that are included in a histogram calculated from all detections. The third column specifies the number of detections that are used to calculate the number density of space objects as a function of orbital parameters. This number is always equal or less than that in the second column, as certain detections are filtered out. Finally,  $\Sigma$  specifies the determined number of space debris objects in the observable diameter, periapsis, and inclination range.

Date	Detections in $m_{r,v,s}$	Detections in fit	$\Sigma \cdot 10^{-5}$
2022-04-05	1227	1227	1.17
2021-11-29	1530	1530	1.41
2021-04-12	1293	1293	1.26
2019-04-02	1392	1389	1.30
2018-01-04	1354	1353	1.30

A list of EISCAT UHF beam park measurements used in this study is found in Table 1. Each observation period is 24 h long. Figure 1 shows a plot of beam-park observation data obtained on 2021-11-29. It shows the debris produced by the Cosmos 1408 anti-satellite missile test [KVGK23]. Figure 2 shows observation data obtained on 2019-04-02. The debris produced by the Microsat-R anti-satellite missile test [Pau21] can be seen.

### 3. METHOD

Radar measurements of space debris are random samples of the population of objects that happen to be detected during a measurement interval by the radar. Modeling the detection correctly as a statistical process is vital for translating the measurements into an estimate of the population of debris. The model can also be used characterize the limitations of the radar, especially in regard to maximal and minimal observable space object parameters. For example, it has been found that a diameter of approximately 1 cm is the smallest possible that can be detected.

A beam park measurement contains a wealth of information about the distribution of objects in space. For example, the detection range carries information about the apogee of an object, the Doppler velocity about the inclination, and the time of observation about the local time of the ascending node. Furthermore, the signal-to-noise ratio and the duration of an observation arc carry information about the diameter of an object. In this study, the Doppler velocity, the signal-to-noise ratio and range at peak signal-to-noise ratio is used.

The relationship between a beam park measurement and the population of objects in space is of statistical nature.

A 24 h beam park measurement detects only  $\approx 1\%$  of all objects with a diameter greater than 0.98 cm and inclination between  $65^\circ$  and  $115^\circ$ . A single detection cannot be used to determine the orbital elements of an object, as the radar measurement is monostatic. However, it is possible to relate the distribution of space objects to the random distribution that generates a beam park measurement, i.e., given a distribution of objects in space, predict what will be the distribution of range, Doppler velocity, and signal-to-noise ratio. This is often called a forward model in the field of statistical inverse problems [ABT18], as this is usually straightforward to do. Simulating the expected number of detections at a given range, Doppler shift, signal-to-noise ratio and time as a function of the density of objects with a certain distribution of orbital element and diameter is such a forward problem. The corresponding inverse problem is estimating the density of space objects as a function of orbital elements, given a beam-park measurement. This is typically a much harder estimation problem, which often requires prior assumptions to be made.

The approach that we will take is to model the number density  $\Lambda$  of measurements with a range ( $r$ ), Doppler velocity ( $v$ ), detection time ( $t$ ), and received signal-to-noise ratio ( $s$ ) during a beam park experiment by

$$\Lambda(r, v, s, t) = \int \rho(\theta) \Psi(r, v, s, t, \theta) d\theta. \quad (1)$$

Here,  $\rho$  is the density of objects with parameters  $\theta$  and  $\Psi$  is a basis function. It provides the expected number of observations of an object specified with parameters  $\theta$  and observed with parameters  $r, v, s, t$ . In our case,  $\theta$  contains the six Keplerian parameters and the diameter  $d$  of the object. The unknown in our case is  $\rho(\theta)$ . The radar sensor model and orbital mechanics determine the function  $\Psi$ .

To make the problem more tractable, it is assumed that  $\rho$  can be written as

$$\rho(\theta) = \rho'(i, p, \Omega) \rho_e(e) \rho_\omega(\omega) \rho_\nu(\nu) \rho_d(d), \quad (2)$$

where  $i$  is the orbital inclination,  $p$  is the periapsis,  $\Omega$  is the local time of the ascending node,  $e$  is the eccentricity,  $\omega$  is the argument of the periapsis and  $\nu$  is the true anomaly. The symbols  $\rho_x$  represent distributions of the variable denoted in the subscript. The assumption (2) means that the random variables  $e, \omega, \nu, d$  are independent of  $i, p, \Omega$  and also independent from each other. Now,  $\rho_\omega$  and  $\rho_\nu$  are assumed to be uniform distributions and  $\rho_e$  and  $\rho_d$  are known prior distributions. Finally, (2) is substituted into (1) and  $\Psi$  is redefined so that the integrals over  $e, \omega, \nu$ , and  $d$  are absorbed. Note that  $\Psi$  now only depends on the difference  $t - \Omega$  modulo the duration of one sidereal day. This means that integrating both sides over  $t$  yields the simplified equation

$$\Lambda'(r, v, s) = \iint \rho''(i, p) \Psi'(r, v, i, p) di dp, \quad (3)$$

where  $\Lambda'$  is equal to  $\Lambda$  marginalized over  $t$ ,  $\rho''$  equals  $\rho'$  marginalized over  $\Omega$  and  $\Psi'$  equals  $\Psi$  marginalized over

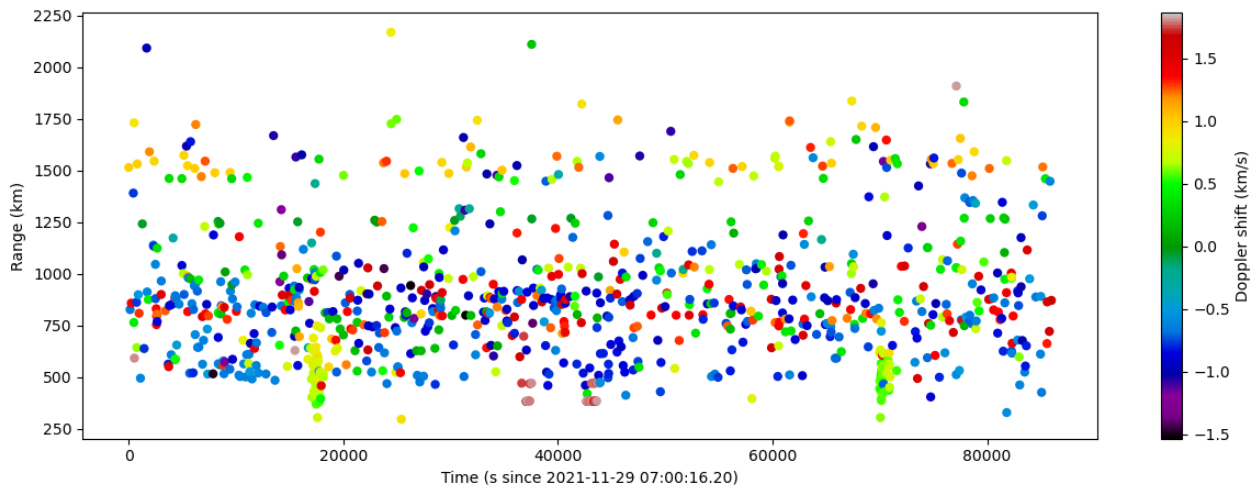


Figure 1. An EISCAT UHF beam park measurement of the Cosmos 1408 anti-satellite missile test debris cloud. The yellow-orange points at approximately 500 km range are objects created by the explosion of the satellite.

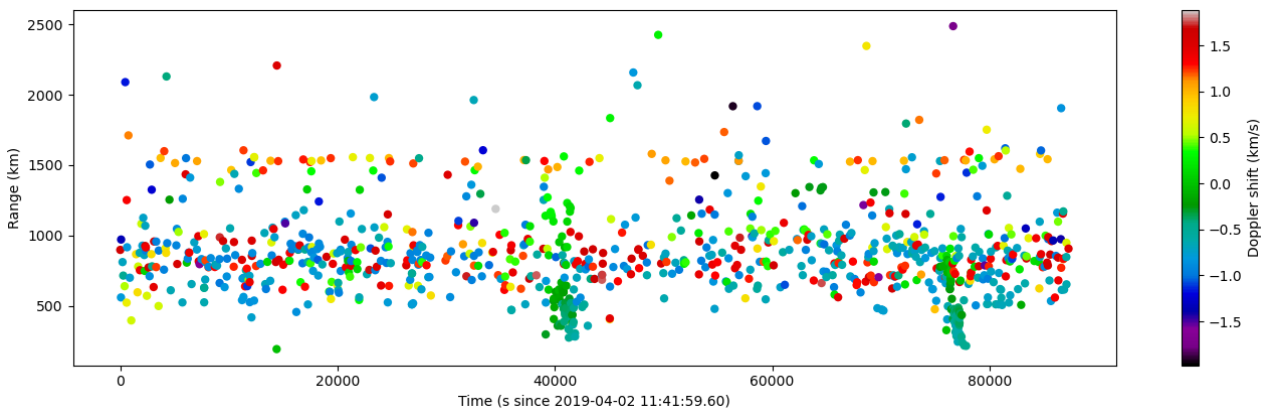


Figure 2. An EISCAT UHF beam park measurement of the Microsat-R anti-satellite missile test debris cloud. The two prominent green-blue clusters of points are objects created by the explosion of the satellite.

$t$ , which essentially removes the  $\Omega$  dependence. This final integration over  $t$  results in a higher bin population of  $\Lambda'$  compared to  $\Lambda$ , but sensitivity on  $\Omega$  is lost. If a lot of statistics are available,  $\rho'$  can also be inferred directly.

In practice, the most straightforward method to calculate  $\Psi'$  is to use a Monte-Carlo approach, where objects with a certain inclination and periapsis are propagated in Earth orbit and measured using a simulated radar [KVK<sup>+</sup>19]. For each object, the remaining parameters  $e, \omega, \nu$ , and  $d$  are randomly drawn from their respective prior distributions.

The  $\rho_d$  and  $\rho_e$  prior distributions are derived from the MASTER 2009 model [FGW<sup>+</sup>09]. The  $\rho_d$  distribution is cut off for  $d < 9.8$  mm, as this is the smallest detectable diameter. It is worth noting that a significant fraction of detectable objects are approximately in a circular orbit.

Discretizing (3) yields

$$\Lambda_{r,v,s} = \sum_{p,i} \rho_{p,i} \Psi_{r,v,s,p,i}, \quad (4)$$

where the sum goes through all of the discretized bins of inclination and periapsis, and the indices  $r, v, s$  are the bin indices of the range, Doppler velocity, and signal-to-noise ratio dimensions, respectively.

It is possible to think of  $\Lambda_{r,v,s}$  as a three-dimensional histogram of range, Doppler, and signal-to-noise detections. It provides the expected number of space debris detections per day, while the space object parameters are distributed according to the priors and  $\rho_{p,i}$ , which is a two-dimensional histogram. Each bin in that histogram describes the total number of space objects with  $d > 0.98$  mm in the bin's respective range of periapsis and inclination values. The histogram  $\rho_{p,i}$  is the unknown that we aim to estimate.

The left-hand side of (4) can now be related to measurements. The measurement data is pre-processed to a three-dimensional histogram of space debris detections as a function of range, Doppler shift and signal-to-noise ratio denoted by  $m_{r,v,s}$ . Figure 3 shows an example of such a histogram, with marginalized  $s$  variable, computed from the 24 h beam park observation made on 2021-11-29.

The number of detections in a histogram bin is a Poisson random variable, as clusters of objects are not considered here. Since some of the objects are detected multiple times, the bins are correlated. In this study, the correlations are neglected. The likelihood function for the estimation of  $\rho_{p,i}$  is given by

$$\mathcal{L} = \prod_{r,v,s} \frac{\Lambda_{r,v,s}^{m_{r,v,s}} \exp(-\Lambda_{r,v,s})}{m_{r,v,s}!}. \quad (5)$$

It is numerically more convenient to minimize the negative logarithm of the likelihood function, which is

$$-\log \mathcal{L} = \sum_{r,v,s} (\Lambda_{r,v,s} - m_{r,v,s} \log \Lambda_{r,v,s}), \quad (6)$$

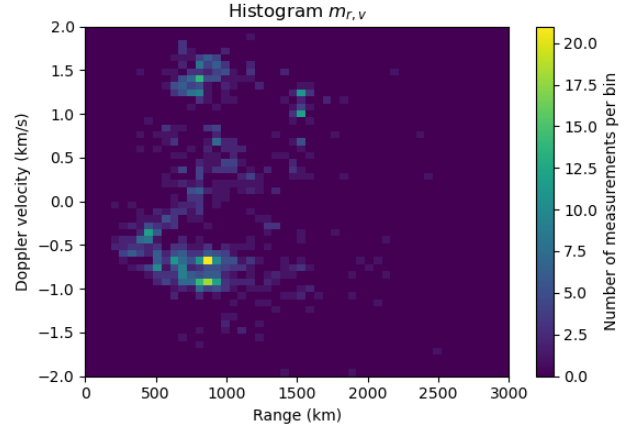


Figure 3. A histogram of detection counts during the 24-hour beam park measurement conducted on 2019-04-02 with the EISCAT UHF radar. This histogram is only a function of range and Doppler. The analysis uses also a third dimension, which is the signal-to-noise ratio.

if constants are discarded.

Finally, we expect a certain level of smoothness within the histogram of object counts, especially for the regions where the number density is very low. It is possible to regularize the solution to encourage smoothness by using  $L_1$ -norm minimization [Rod13]. This can be seen as a prior assumption of the smoothness of our unknown:

$$-\log p_{\text{MAP}} = \sum_{r,v,s} (\Lambda_{r,v,s} - m_{r,v,s} \log \Lambda_{r,v,s}) + \lambda \sum_{p,i} (|\rho_{p,i} - \rho_{p,i+1}| + |\rho_{p,i} - \rho_{p+1,i}|). \quad (7)$$

Here the constant  $\lambda \geq 0$  is a parameter that determines how smooth the solution is assumed to be. Another prior information that was used is  $\rho_{p,i} \geq 0$ .

The minimum value of (7), which corresponds to the maximum a posteriori estimate of  $\rho_{p,i}$ , is obtained numerically. For that, the non-linear optimization algorithm L-BFGS-B [ZBLN97] is used.

It can happen that the expected number of detections in some  $r, v, s$  bin becomes exactly zero, while the measured number of detections in that bin is not zero. This contradiction between measurement and model has only been observed for some measurements. It is currently overcome by excluding such bins from the optimization. This results in a smaller number of events that are actually taken into account in the fit, see Table 1.

## 4. RESULTS

Figure 4 shows the estimated distribution functions  $\rho_{p,i}$  for the different beam park measurements. The promi-

ment peak at just below  $100^\circ$  inclination and ranging from approximately 500 km up to 900 km periapsis corresponds to the highly populated sun-synchronous orbits at  $97.7^\circ$  inclination and 567 km altitude, as well as  $99^\circ$  inclination and 894 km altitude. This cluster is depicted with red box number 1 in the lower right panel. Another highly populated sun-synchronous orbit at  $103^\circ$  inclination and 1681 km altitude can also be seen, denoted with a red box and a number 2. Note that the extent of inclinations that can be inferred from the data is limited by the high latitude location of the radar ( $69^\circ N$ ).

By inspecting the evolution of the distribution over time between 2018 and 2022, it is possible to see the appearance of new clusters during fragmentation events. For example, on 2019-04-02 there is a cluster caused by the Microsat-R anti-satellite missile test, and in the 2021-11-29 and 2022-04-05 measurements there is a new cluster caused by the Cosmos 1408 anti-satellite missile test. Note that the shape of the Microsat-R cluster is not compact. One possible explanation for this is that the prior distribution of eccentricities is not applicable to the cluster. The prior assumes that most objects have low eccentricities, while it can be seen in Figure 2 that some objects in the cluster have high eccentricities. This causes the density estimation to erroneously include densities with higher values of periapsis for the cluster.

## 5. DISCUSSION

In order to compare these results with a model, a comparison plot with identical inclination and periapsis binning as well as object diameter limits is computed using the MASTER 2009 model (see Figure 5). Qualitative agreement in the morphology of  $\rho_{p,i}$  and the model can be seen.

The total counts  $\Sigma$  estimated from the beam park measurements are higher by a factor of approximately 2.4. Note that the number of cataloged objects in LEO is estimated to have grown by about this factor since 2008 [Off22].

Table 1 shows that from 2018 to 2021 the total number of space debris objects stayed approximately constant, followed by an increase in the year 2021. However, the expected upwards trend is not continued with the measurement on 2022-04-05. This is likely to blame on a technical issue during the measurement: the radar signal generator run with an unlocked oscillator. This caused a loss of sensitivity that is not easy to characterize and not considered when estimating the density function. The estimated density on 2022-04-05 is thus likely to be an underestimate of the total amount of debris.

## 6. CONCLUSIONS

The density function estimation technique introduced in this study was shown to provide robust estimates of the distribution of space debris as a function of periapsis and inclination. The estimated number density agrees well in morphology with the ESA MASTER 2009 model. However, work is needed in order to verify the validity of this proof-of-concept study.

While we did not explore the use of other choices of marginalization, it is straightforward to extend the presented technique to estimate the three-dimensional distribution of periapsis, inclination, and longitude of the ascending node. In this case, three-dimensional histograms with detection time, range, and Doppler shift could be used for the histogram of the measured data.

The three-dimensional histogram of range, signal-to-noise ratio and event duration includes information about the object diameter distribution  $\rho_d$ . Incorporating event duration to constrain  $\rho_d$  will be explored in future work. Another source of information about  $\rho_d$  is the distribution of unbiased radar cross-section measurements. Incorporating such information would be possible with this framework as well. Current EISCAT measurements unfortunately do not contain unbiased radar cross-section measurements, but future EISCAT 3D measurements will [KKV<sup>+</sup>19].

For this study, we did not take known cataloged objects into account. Considering these objects might result in less uncertainty for the estimated density, as large objects in side lobes of the radar antenna account for a significant fraction of detections [VKM<sup>+</sup>19] in beam park measurements.

## AUTHOR CONTRIBUTIONS

The author's contributions are as follows: JV, FH, and DK came up with the idea, FH implemented the estimation method and wrote the first draft of the manuscript, JM analyzed the beam park measurements and JV, DK, JK, JM and TG conducted the beam park measurements. All authors contributed to the manuscript.

## ACKNOWLEDGMENTS

We thank the EISCAT staff for making these measurements possible. JV acknowledges financial support from the Tromsø Science Foundation. All authors acknowledge support from the ESA Space Debris Office.

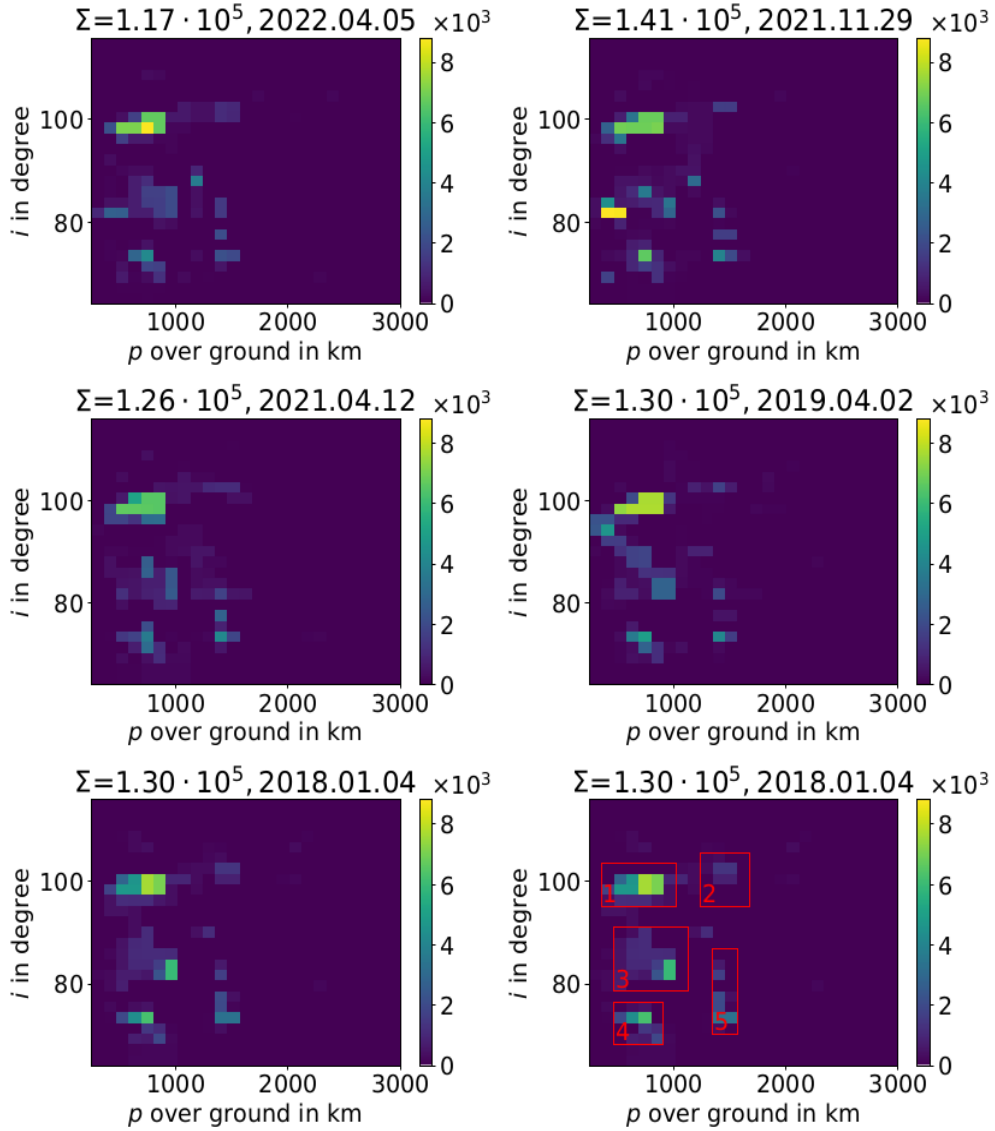


Figure 4. Estimated space debris distributions  $\rho_{p,i}$  over periapsis  $p$  and inclination  $i$ . Each bin specifies the estimated number of space objects with a diameter  $>0.98$  cm in the bin's respective periapsis and inclination range. The date of the beam park measurement is stated in the plot titles as well as the total number  $\Sigma$  of objects (sum over all bins). The bottom-right plot is the same as the bottom-left plot, but with boxes drawn around five different clusters of objects.

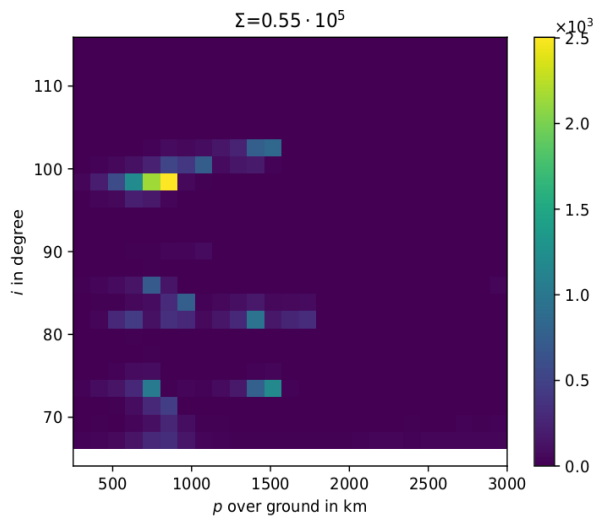


Figure 5. The space debris distribution  $\rho_{p,i}$  obtained from the MASTER 2009 model, using the same inclination and periastron binning, as well as the same minimum diameter as the analysis. In the plot title,  $\Sigma$  denotes the total number of objects (sum over all bins).

## REFERENCES

- ABT18. Richard C Aster, Brian Borchers, and Clifford H Thurber. *Parameter estimation and inverse problems*. Elsevier, 2018.
- BHL<sup>+</sup>21. V Braun, A Horstmann, S Lemmens, C Wiedemann, and L Böttcher. Recent developments in space debris environment modelling, verification and validation with MASTER. In *8th European Conference on Space Debris*, 2021.
- FGW<sup>+</sup>09. S Flegel, J Gelhaus, C Wiedemann, P Vorsmann, M Oswald, S Stabroth, H Klinkrad, and H Krag. The master-2009 space debris environment model. In *Fifth European Conference on Space Debris*, volume 672, pages 1–8. European Space Agency/European Space Operations Centre Darmstadt, Germany, 2009.
- KBKB<sup>+</sup>00. H Krag, P Beltrami-Karlezi, J Bendisch, H Klinkrad, D Rex, J Rosebrock, and T Schildknecht. PROOF—The extension of ESA’s MASTER Model to predict debris detections. *Acta Astronautica*, 47(2-9):687–697, 2000.
- KKV<sup>+</sup>19. Johan Kero, Daniel Kastinen, Juha Vierinen, Tom Grydeland, Craig J Heinselman, Jussi Markkanen, and Anders Tjulin. Eiscat 3d: the next generation international atmosphere and geospace research radar. 2019.
- KVGK23. Daniel Kastinen, Juha Vierinen, Tom Grydeland, and Johan Kero. Using radar beam-parks to characterize the Kosmos-1408 fragmentation event. *Acta Astronautica*, 202:341–359, 2023.
- KVK<sup>+</sup>19. D Kastinen, Juha Vierinen, Johan Kero, S Hesselbach, Tom Grydeland, and Holger Krag. Next-generation Space Object Radar Tracking Simulator: SORTS++. 2019.
- LJF04. Markus Landgraf, R Jehn, and W Flury. Comparison of EISCAT radar data on space debris with model predictions by the master model of ESA. *Advances in Space Research*, 34(5):872–877, 2004.
- MJK09. J Markkanen, R Jehn, and H Krag. EISCAT space debris during the IPY—a 5000 hour campaign. In *Proc. 5th ESA space debris conference*, volume 625, 2009.
- MLL05. Jussi Markkanen, Markku Lehtinen, and M Landgraf. Real-time space debris monitoring with EISCAT. *Advances in space research*, 35(7):1197–1209, 2005.
- MMP<sup>+</sup>21. Giacomo Muntoni, Giorgio Montisci, Tonino Pisanu, Pietro Andronico, and Giuseppe Valente. Crowded space: a review on radar measurements for space debris monitoring and tracking. *Applied Sciences*, 11(4):1364, 2021.
- Off22. Space Debris Office. ESA’s annual space environment report. Technical report, Technical Report GEN-DB-LOG-00288-OPS-SD, ESA, 2022.
- Pau21. Martinius Ekeland Paulsen. Radar observations of space debris in polar orbits 2018–2021. a study on the evolution of the Microsat-R fragments. Master’s thesis, UiT Norges arktiske universitet, 2021.
- Rod13. Paul Rodríguez. Total variation regularization algorithms for images corrupted with different noise models: a review. *Journal of Electrical and Computer Engineering*, 2013, 2013.
- SKT<sup>+</sup>95. EG Stansbery, DJ Kessler, TE Tracy, MJ Matney, and JF Stanley. Characterization of the orbital debris environment from haystack radar measurements. *Advances in Space Research*, 16(11):5–16, 1995.
- VKM<sup>+</sup>19. Juha Vierinen, D Kastinen, Jussi Markkanen, Tom Grydeland, Johan Kero, A Horstmann, S Hesselbach, C Kerschull, Elisabeth Røynestad, and Holger Krag. 2018 beam-park observations of space debris with the EISCAT radars. 2019.
- VMK09. Juha Vierinen, Jussi Markkanen, and Holger Krag. High power large aperture radar observations of the Iridium-Cosmos collision. In *Proc. 5th ESA space debris conference*, 2009.
- ZBLN97. Ciyou Zhu, Richard H Byrd, Peihuang Lu, and Jorge Nocedal. Algorithm

778: L-BFGS-B: Fortran subroutines for large-scale bound-constrained optimization. *ACM Transactions on mathematical software (TOMS)*, 23(4):550–560, 1997.